RESEARCH ARTICLE | SEPTEMBER 08 2023

Green production and analysis of silver nanoparticles utilizing Pathor Kuchi Leaf

N. Y. Tanisa ; Md Kamrul Alam khan ; M. Salahuddin

AIP Advances 13, 095010 (2023)
https://doi.org/10.1063/5.0162169

Green production and analysis of silver nanoparticles utilizing Pathor Kuchi Leaf

Cite as: AIP Advances 13, 095010 (2023); doi: 10.1063/5.0162169
Submitted: 14 June 2023 • Accepted: 21 August 2023 •
Published Online: 8 September 2023

N. Y. Tanisa,[1,2,a)] Md Kamrul Alam khan,[3] and M. Salahuddin[2]

AFFILIATIONS

[1] Department of Physics, Uttara University, Uttara, Dhaka 1230, Bangladesh
[2] Department of Physics, Jahangirnagar University, Dhaka 1340, Bangladesh
[3] Department of Physics, Jagannath University, Dhaka 1100, Bangladesh

[a)] **Author to whom correspondence should be addressed:** tanisha.90@uttarauniversity.edu.bd

ABSTRACT

Silver nanoparticles (Ag NPs) were manufactured utilizing Pathor Kuchi Leaf (PKL) extract in an environmentally, cost-effective green way. X-Ray Powder Diffraction (XRD), Fourier Transform Infrared (FTIR), Ultraviolet–Visible Spectroscopy (UV–Vis), and Scanning Electron Microscopy (SEM) have been used to look into Ag NPs generation. The crystalline structure was shown by the XRD pattern investigation, and its typical size is 19 nm. Its biological molecules composites are in charge of the diminishment and also the capping of Ag NPs, according to FTIR spectra. The UV–Vis spectra of silver NPs expressed a noticeably large absorption peak centered at ~400 nm, which denoted the production of Ag^0 from Ag^+. After the distribution of sizes analysis, it must have been discovered that the mean dimension of the particles of the spherical silver nanoparticles in the SEM pictures was 5.33 μm. Ag NPs have been shown to potentially improve the power generation, short circuit current, and open circuit voltage of PKL bio-electrochemical cells. This work exhibits a straightforward, economical, and ecologically friendly way of manufacturing. The uniqueness of this work is that it is the first-ever comparative analysis of Ag NPs' production utilizing PKL extract. The majority of the conclusions have been grouped and visually explained.

I. INTRODUCTION

Current advancements in PKL power have been focused on in prior studies[1,2] and have attracted broad attention. Because of their distinctive morphologies, stability, and regulated geometry, Ag NPs have drawn a significant amount of attention.[3] It is believed that the activity of zinc metal with PKL juice as the major material, Pathor Kuchi Leaf juice including many organic acids, is the key material.[4–6] Because of their unique properties and diverse applications in numerical areas such as engineering, optoelectronics, and bioimaging,[7–14] nanoparticles have been extensively researched over the last few decades. Noble metal nanoparticles (e.g., platinum, gold, and silver)[15] are widely employed in transdisciplinary disciplines such as substantial, synthetical, technical, and nuclear applications.[7,10] A novel technology called nanotechnology has produced major improvements in a number of industries. Due to their unique prospective applications in the fields of electrical,[16] magnetic,[17] and optoelectronics,[18] metal NPs' production has recently attracted significant research attention in modern material science. Ag NPs have distinct physical and chemical features that make them remarkable in a range of applications and have caught the interest of various researchers.

The extraordinary physiochemical characteristics of silver nanoparticles, which create these values in a range of applications, have caught the interest of various researchers. A number of various plant preparations have been used to effectively create Ag NPs. Among the plant extracts employed are those from the leaves of *Cinnamomum camphora*,[19] *Aloe vera*,[20] *Allium sativa* (garlic),[21] *Capsicum annum* (pepper),[22] etc. Furthermore, Ag NPs' applications have expanded quickly as a result of their enormous impacts on targeted medicine delivery, the food and beverage sectors, water treatment, and textiles.[23,24] Numerous chemical processes have been used to create Ag NPs, and these processes have been reported in the literature to date.[25] Using fruit and vegetable extracts might be beneficial in a different way to get rid of harmful substances that were left behind after synthesizing NPs, which might hasten their use in

medical applications.[15] Numerous vital substances such as polyphenols, terpenoids, ascorbic acids, and alkaloids, may be crucial to the process of removing metal ions from precursor solutions, and NPs can be encased as biological molecules.[15,26,27] Currently, research is being conducted on the green synthesis of silver nanoparticles using the leaf extract of the medicinal plant *Uvaria narum* and its antibacterial, antiangiogenic, anticancer, and catalytic properties.[28–30] Reported on the green synthesis of silver nanoparticles using extracts of *Jasminum officinal L.* leaves and the evaluation of cytotoxic activity toward bladder (5637) and breast cancer (MCF-7) cell lines.

However, further research is still needed to fully understand how green synthesized NPs may be used in the production of power. In this work, Ag NPs were created using PKL extract, and their electrical properties were examined in relation to bio-electrochemical cells used in power production systems. In that piece of work, we presented the outcomes of using Ag NPs synthesized from PKL in a comparative study independently as a reducing agent.

In this work, the power development of PKL extract-based Zn/Cu electrochemical cells employing Ag NPs has been explored. The reduction of Ag^{+} to Ag^{0} atoms was accomplished by the existing functional group of PKL extract during the synthesis of Ag NPs. An evaluation of a PKL bio-electrochemical cell with and without Ag NPs has been performed. The effects of Ag NPs on the enhancement of power generation have been researched in relation to several electrical parameters of the cells. When introducing Ag NPs into bio-electrochemical cells, the open circuit voltage and short circuit current increased with time. As a consequence, the power generation of the targeted cells has been greatly enhanced. This research will improve the usage of Ag NPs in power generation for energy development purposes.

II. MATERIALS AND METHODS

A. Pathor Kuchi Leaf extract preparation

The nearby nursery was where the pure PKL was obtained. To minimize dust particles, the obtained PKL was carefully cleaned. To reduce dust particles, clean PKL using a water supply and deionized (DI) water, then dry at room temperature. The dried washed PKL was mashed to make an extract with grindstones. 25 g of the extract of PKL was merged with 125 ml of de-ionized water and then shaken using a magnetic stirrer with a hot plate heated at 62 °C for 60 min. After making it cool at normal (room) temperature, the PKL extract

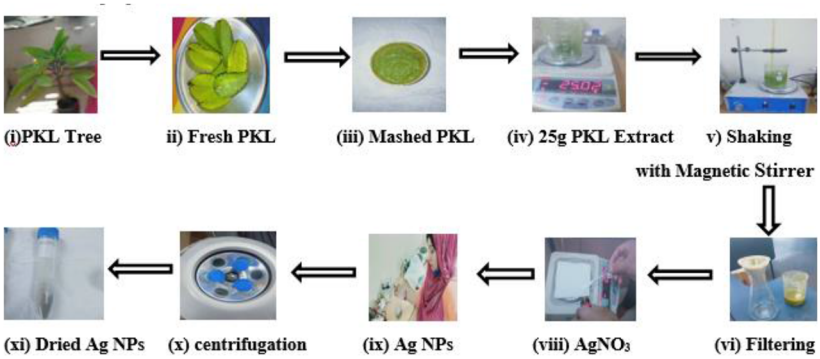

FIG. 1. Displays a graphic depiction of Ag NPs generation.

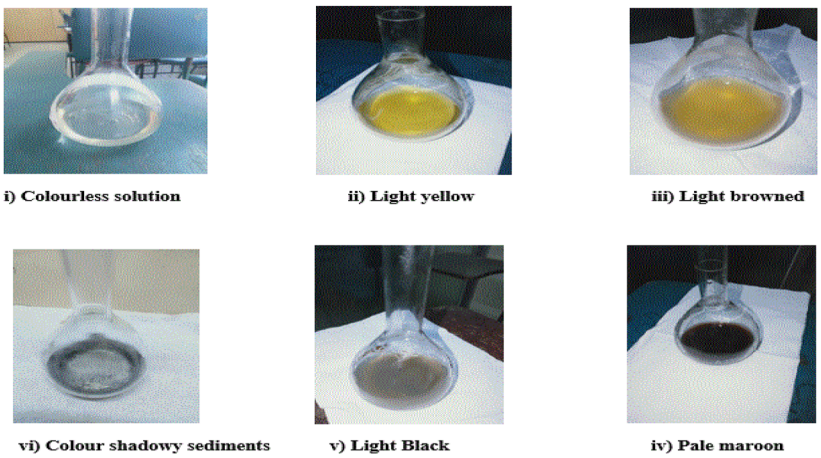

FIG. 2. The color-changing diagram of synthesized silver NPs.

was obtained by filtering the mixture once with Whiteman 42 paper to reduce residual solids and storing it at 4 °C for 60 min.[31]

B. Formation of Ag nanoparticles using Pathor Kuchi Leaf

In order to create Ag NPs, 5 and 7 ml of PKL-filtered extract were added separately to 45 ml of 1 mM $AgNO_3$ solution. Then, after putting it under light for further analysis, after 1 h, the colorless solution shifted from light yellow to pale maroon. Within a few days, it was finally possible to create a light black color of shadowy sediments near the bottom of the flask's solution, which in turn affirmed the manufacturing of Ag NPs. After that, the manufactured Ag NPs were identified by centrifugation[32] at 3000 rpm[32] seven times for 1 h. Then, the centrifuged particles were washed with de-ionized water and again subjected to centrifugation[32,33] at 3000 rpm for 5 min. Separated Ag NPs were dried on a hot plate. The calcites Ag NPs were used for further analytical techniques. Figure 1 shows a graphic depiction of Ag NPs' generation, and Fig. 2 shows the color-changing diagram of synthesized silver NPs.

C. Identification of green synthesis of Ag NPs

The x-ray powder diffraction pattern of Ag NPs in powder form was investigated. The prepared sample was pressed onto an optically clear glass plate in a (40 × 40 mm^2) rectangular aluminum specimen holder with a square hole that really was 1 mm deep (20 × 15 mm^2). With its specimen holder, the sample's top surface was identified on the plane. After that, the specimen holder is inserted into the diffractometer. XRD analysis of the crystalline structure of silver NPs [X-Ray Diffractometer (PW3040), Philips Pan Analytical Co., Ltd., The Netherlands]. The CuKα rays (λ = 1.5405 Å) have been recognized and employed for X-ray powder diffraction readings in a variety limited to 2θ angle (10°–80°). With dry and pure KBr crystals, FTIR studies of silver NPs manufactured by PKL extraction were carried out on the IRPrestige-21 in Kyoto, Japan, at a 4.0 cm^{-1} determination. UV–Vis variants are based on the concept that chemical compounds absorb ultraviolet or visible light, creating unique spectra in the process. The interaction of light and matter is the foundation of spectroscopy. Utilizing a UV–Vis (UV-1700, Kyoto, Japan), the University of Dhaka's Center for Advanced Research in Sciences (CARS) analyzed the reaction solution's spectrum 2- to 3-fold diluted to investigate the creation of silver nanoparticles. Scanning electron microscopy (SEM) pictures were used to investigate the morphology of silver nanoparticles.

D. Bio electrochemical cells principles

Using Zn and Cu plates as electrodes, PKL extract as an electrolyte, and green-produced silver nanoparticles as a catalyst, a Zn/Cu-BPL bio-electrochemical cell was created (shown here in Fig. 3). Therefore, in the cell, the electrons are lost by the zinc plate, gained by the copper plate, and then reacted with H^+ and Cu^{2+} ions. Ions are gradually converted into H_2 and Cu atoms, respectively.

E. Bio electrochemical effective channel

To examine the effects of Ag NPs on the system that produces electricity, three distinct bio-electrochemical cells were built. In Example 1, Zn and Cu plates with similar surface areas were employed as electrodes. As the cell's electrolyte, 125 ml of BPL extract and 6 ml of 0.4006M $CuSO_4 \cdot 5H_2O$ solution were utilized. The cell's electrolyte solution was then supplemented with a 15 ml solution of Ag NPs. As electrodes in Example 2, Zn and Cu plates were employed. To create the electrolyte for Example 2, 125 ml of PKL extract and 6 ml of 0.4006M $CuSO_4 \cdot 5H_2O$ were combined. As for the electrolyte in Example 3, just 125 ml of PKL extract was used. The basic idea of Zn/Cu-based BPL bio-electrochemical cells is shown experimentally in Fig. 3.

III. RESULTS AND DISCUSSION

A. XRD studies

The spatial characterization of PKL extract-mediated green synthesized silver NPs was carried out using the X-Ray Diffraction (XRD) technique.[34] In Fig. 4(i), the diffracted images for the synthesized Ag NPs for 7 ml PKL were obtained at Bragg's angles of 38°, 44°, 65°, and 78°, which were indexed to (111), (200), (220), and (311) planes (JCPDS No. 65-2871).[8,11,14,24,27,35–40] In Fig. 4(ii), the diffracted images for the synthesized Ag NPs for 5 ml PKL were obtained at Bragg's angles of 38°, 44°, 65°, and 78°, which were indexed to (111), (200), (220), and (311) planes (JCPDS No. 65-2871).[8,11,14,24,27,35–40] In Fig. 4(iii), the diffracted images for the PKL extract were obtained at Bragg's angles of 38°, 45°, 66°, and 79°,

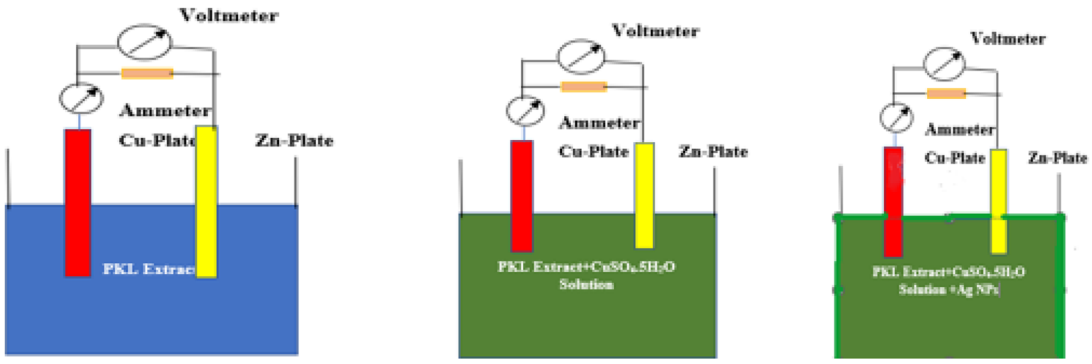

FIG. 3. The basic idea of Zn/Cu-based BPL bio-electrochemical cells is shown experimentally.

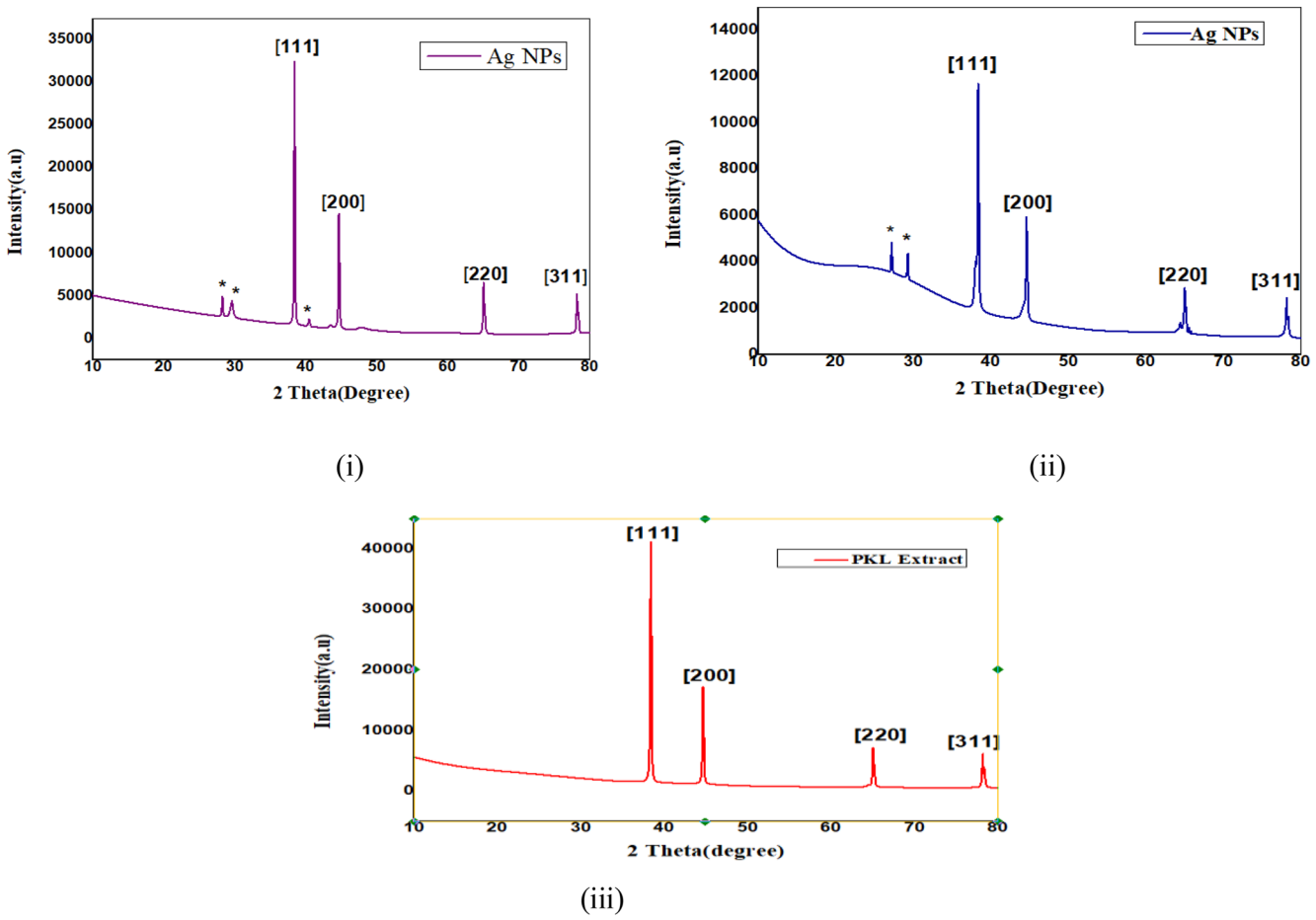

FIG. 4. (i) Intensity vs 2θ for synthesized Ag NPs for 7 ml; (ii) intensity vs 2θ for synthesized Ag NPs for 5 ml; and (iii) intensity vs 2θ for PKL extract.

which were indexed to (111), (200), (220), and (311) planes (JCPDS No. 65-2871).[8,11,14,24,27,35–40] For the cubic structure of AgK_3,[15] an extreme peak at 38° may have formed.[19]

By applying the Scherrer equation to the XRD pattern,[38] the particle size can be calculated,

$$D = K\lambda/(\beta \cos\theta),$$

where D is the mean size of crystallites (nm), K is the crystallite shape factor (a good approximation is 0.9), λ is the x-ray wavelength, β is the full width at half the maximum (FWHM)[41–44] in radians of the x-ray diffraction peak, and θ is the Braggs' angle (deg).[41] The average crystal size of the green-produced silver NPs is reported to be 19 nm. The XRD analysis showed some noticeable peaks, and many papers obtained comparable results.[45–51] The XRD pattern included some noticeable highs (indicated with *), and many papers obtained consistent outcomes.[46–51]

B. FTIR studies

Various functional groups of various chemicals discovered in plant extracts (such as polyphenols, polysaccharides, flavonoids, and triterpenoids) are in charge of clearing the forerunner of metal oxide nanoparticles[15] sodium chloride.[18] The stretching, wagging, and bending vibrations of these functional groups[19] and the capping and reducing of nanoparticles may be closely related operations.[15] FTIR interpretation is accustomed to exploring functional groupings that might be at fault for the reducing, capping, and effectively stabilizing of filtered PKL extract, $AgNO_3$ dissolved in de-ionized water, and PKL extract-mediated Ag NPs. Figure 5(i) illustrates the FTIR absorption spectra of PKL extract-mediated Ag NPs for 7 ml PKL. The spectra indicated a number of peaks around 536, 1200, 1324, 1628, 2118, and 3320 cm^{-1}. From this result, it was discovered that PKL extract-mediated Ag NPs for 7 ml PKL had the highest peak of 3320 cm^{-1} with the O–H stretching vibration functional group. A peak at around 536 cm^{-1} was possibly connected to the vibrational stretching of the CO[15] bond, whereas the peak at around 1200 cm^{-1}

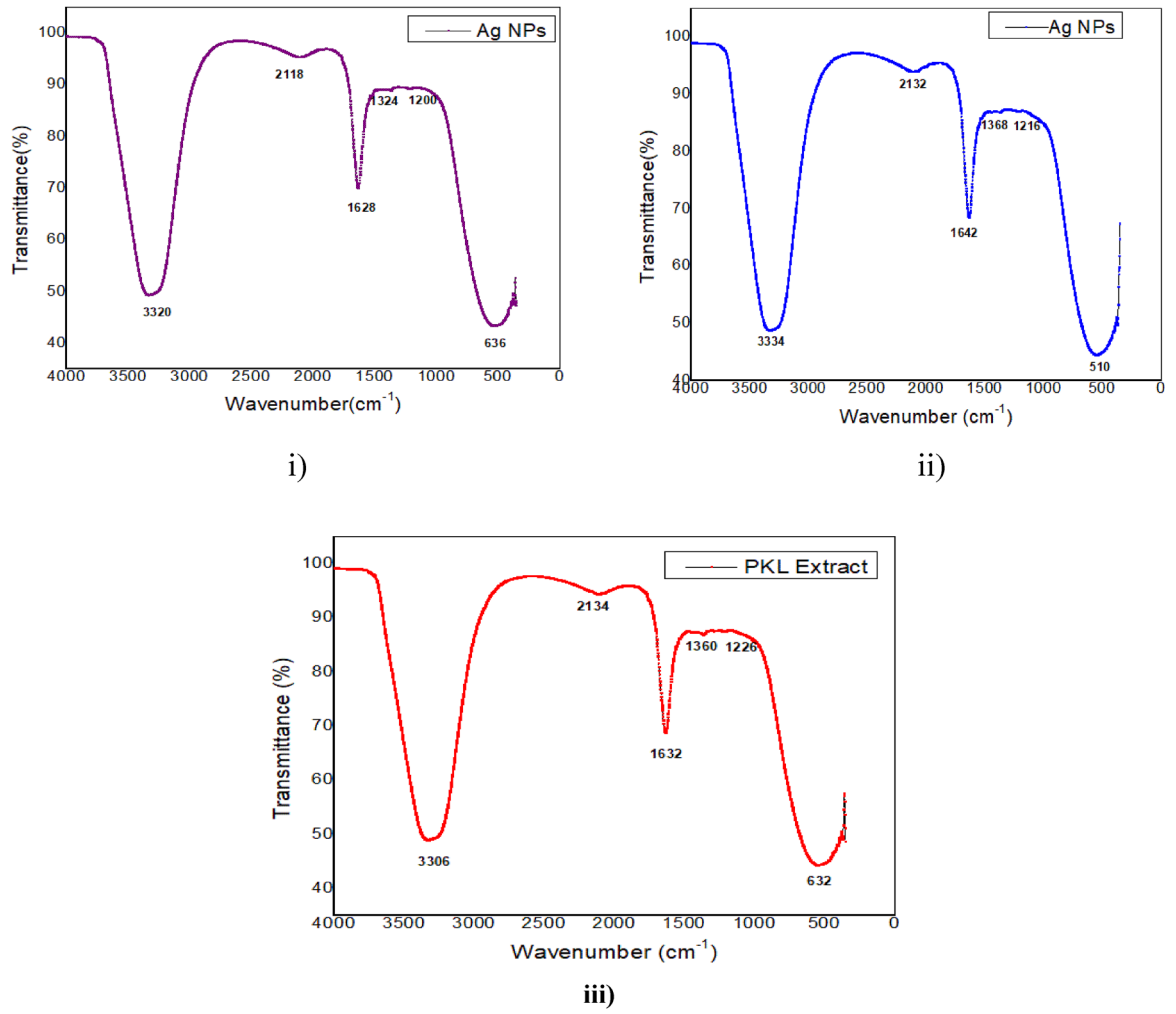

FIG. 5. (i) FTIR of PKL extract mediated Ag NPs for 7 ml; (ii) FTIR of PKL extract mediated Ag NPs for 5 ml PKL; and (iii) PKL FTIR of filtered PKL extract.

appeared due to the bending of the O–H bond. A significant peak at 1324 cm^{-1} is assigned to the nitrogen compounds stretching their N–O bonds.[3] Furthermore, the heights at ~1628 and 2118 cm^{-1} appeared due to the stretching vibration of C=C and C=O bonds, respectively.[52] Another high peak that occurs at around 3320 cm^{-1} is the result of the bending vibration of C≡C, the bond of alkyne.[11] Figure 5(ii) illustrates the FTIR spectra of PKL extract-mediated Ag NPs for 5 ml PKL. The spectra indicated a number of peaks around 510, 1216, 1368, 1642, 2132, and 3334 cm^{-1}. From this result, it was discovered that PKL extract-mediated Ag NPs for 5 ml PKL had the highest peak of 3334 cm^{-1} with the O–H stretching vibration functional group. The peak at around 510 cm^{-1} was possibly connected to the vibrational stretching of the CO[15] bond, whereas the peak at around 1216 cm^{-1} appeared due to the bending of the O–H bond. A significant peak at 1368 cm^{-1} is assigned to the N–O stretching of nitro compounds.[3] Furthermore, the peaks at around 1642 and 2132 cm^{-1} appeared due to the stretching vibration of C=C and C=O bonds, respectively.[52] Another high peak that occurs at around 3334 cm^{-1} is the result of the bending vibration of C≡C, the bond of alkyne.[11] Figure 5(iii) illustrates the FTIR spectra of the PKL extract. The spectra indicated a number of peaks around 532, 1226, 1380, 1632, 2114, and 3308 cm^{-1}. From this result, it was discovered that PKL extract-mediated Ag NPs had the highest peak of 3308 cm^{-1} with the O–H stretching vibration functional group. The peak at around 632 cm^{-1} was possibly connected to the vibrational stretching of the CO[15] bond of alkyl aryl ether. The peak at 1226 cm^{-1} may be caused by the bending of the O–H bond. Furthermore, the heights at ~1380 cm^{-1} appeared due to the stretching vibration of C=C.[3] Another high peak that occurs at around 2114 cm^{-1} is the result of the bending vibration of the C≡C bond. Moreover, the peak at wave number 3308 cm^{-1} may have appeared due to the O–H and N–H stretching.[11]

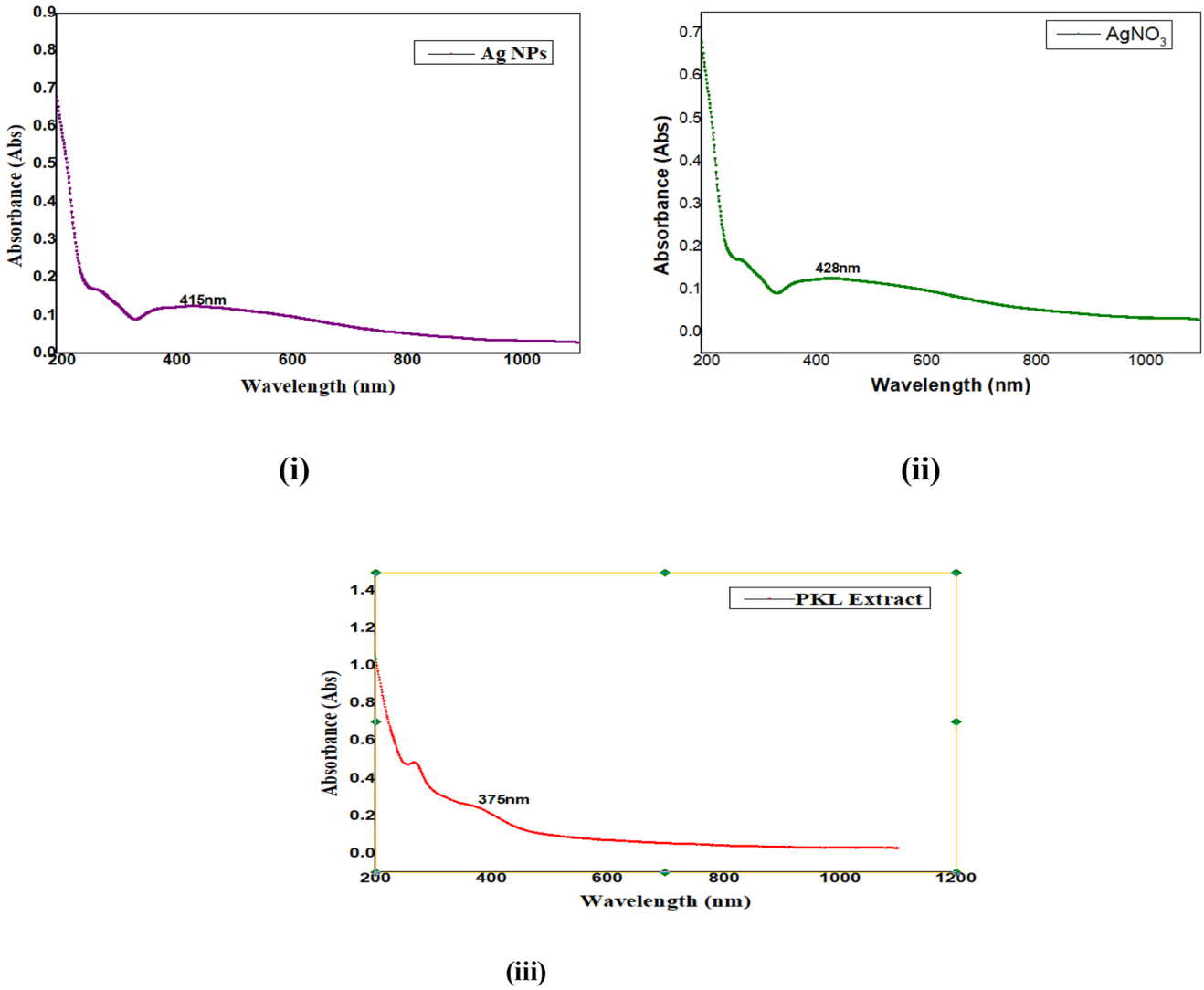

FIG. 6. (i) UV–Vis spectra of Ag NPs for 7 ml PKL; (ii) UV–Vis spectra for $AgNO_3$; and (iii) UV–Vis spectra for filtered PKL extract.

C. UV-visible spectra studies

In the UV-visible spectrum, Fig. 6(i) reveals a sharp peak at around 415 nm, which appeared due to the band emission of Ag NPs for 7 ml PKL. Adding PKL extract to the $AgNO_3$ solution throughout the synthesis method caused the solution's color to shift to shadowy, indicating the creation of Ag^0 from the $AgNO_3$ solution. The reductant of plant extract was critical in the oxidation of Ag.[50]

On the other hand, Fig. 6(ii) shows the UV–Vis spectra of $AgNO_3$ salt solution in DI water (green line). The green line reveals a sharp peak at around 428 nm. Figure 6(iii) shows the UV–Vis spectra of PKL extract (red line). The red line did not appear to have any particular peak at a total of 300 to 900-nm wavelengths.

D. Scanning electron microscopy studies

The SEM examination assessed the morphology or form of the produced Ag nanoparticles. The microscopic pictures of the Ag nanoparticles mediated by PKL extract are shown in Fig. 7 and clearly depict their distribution and spherical form for both the 7 and 5 ml PKL under study. It was found that the particle sizes were the same for both the 7 and 5 ml synthesized PKL Ag NPs.

E. Power generation activities for bio-electrochemical cell

Green-produced Ag NPs were used in a bio-electrochemical cell to investigate the function of NPs in the power generation

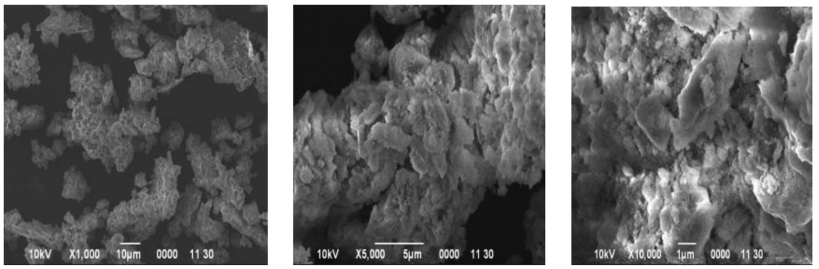

(i)

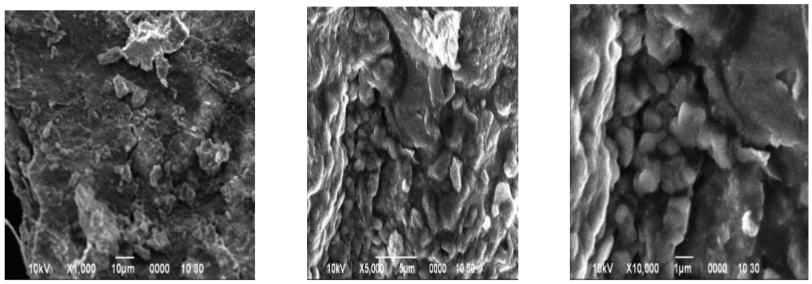

(ii)

FIG. 7. (i) SEM pictures of synthetic Ag NPs in various sizes were created by 7 ml PKL, and (ii) SEM pictures of synthetic Ag NPs in various sizes were created by 5 ml PKL.

system. Green-produced Ag NPs were used in a bio-electrochemical cell to investigate the function of NPs in the power generation system. Ag NPs' effects on three bio-electrochemical cells are shown in Fig. 7. In Fig. 8(i), the open circuit voltage is depicted together with various time duration variations for various scenarios. The open circuit voltages for scenario 1 are demonstrated to be greater than those for scenarios 2 and 3. It's worth noting that the voltage in scenario 1 was practically constant for 70 h. In the first scenario, the highest voltage is 1 V and the minimum is 0.92 V. The highest open circuit voltage for scenario 2 is 0.99 V, and the minimum voltage is 0.88 V; for just PKL extract (Scenario 3), the maximum voltage is 0.98 V, while the minimum voltage is 0.87 V. The highest difference in open circuit voltage between the first and second scenarios is 0.01 V. The difference in open circuit voltage between the first and third cases is 0.02 V, whereas the difference between the second and third cases is 0.01 V. The results indicated that the biggest variation in open circuit voltage discovered is 0.01 V, indicating that nanoparticles may have a role in boosting open circuit voltage. The short circuit current is displayed in Fig. 8(ii), together with varying time durations for various scenarios. It is amply proved that scenario 1 has a greater short circuit current than scenarios 2 and 3. It can be deduced that, when compared to the other two examples, scenario 1 produces the highest short circuit current (40 mA), and it stayed constant for 70 h. Scenario 1 has a minimal short circuit current value of 40 mA, which is higher than the values for scenarios 2 and 3 (all of which are 36 mA) (19 mA). Furthermore, it is clear that Ag NPs may contribute significantly to raising the PKL bio-electrochemical cell's short circuit current over time. Figure 8(iii) depicts the estimated power of the cells with time. The maximum power for scenario 1 is expected to be 40 W, while the minimum power value is 24 W. Scenario 2 and scenario 3 have the most power at 35 and 19 W, respectively, and the lowest power at 20 and 17 W, respectively. The greatest power is discovered after adding the Ag NPs to the PKL bio-electrochemical cell, which is also stable for the following 70 h. Internal resistance is seen in Fig. 8(iv) for all three examples. Only PKL extract bio-electrochemical cells had greater internal resistance than the other two situations. Internal resistance dropped fast after employing the secondary salt solution ($CuSO_4 \cdot 5H_2O$) in scenario 2 and Ag NPs in scenario 1. The open circuit voltage and short circuit current are quickly enhanced after adding the Ag NPs to the cell. As a consequence, the PKL bio-electrochemical cell's power is greatly boosted. In contrast, the internal resistance was found to be ~0.155 Ω for the PKL extract alone, and it unexpectedly decreased to around 0.025 Ω for the bio-electrochemical cell (PKL + $CuSO_4$ solution). After introducing NPs to the cell, the resistance dropped to 0.0125 Ω. It is anticipated that the effects of Ag NPs in the bio-electrochemical cell will be notable for applications in future power growth.

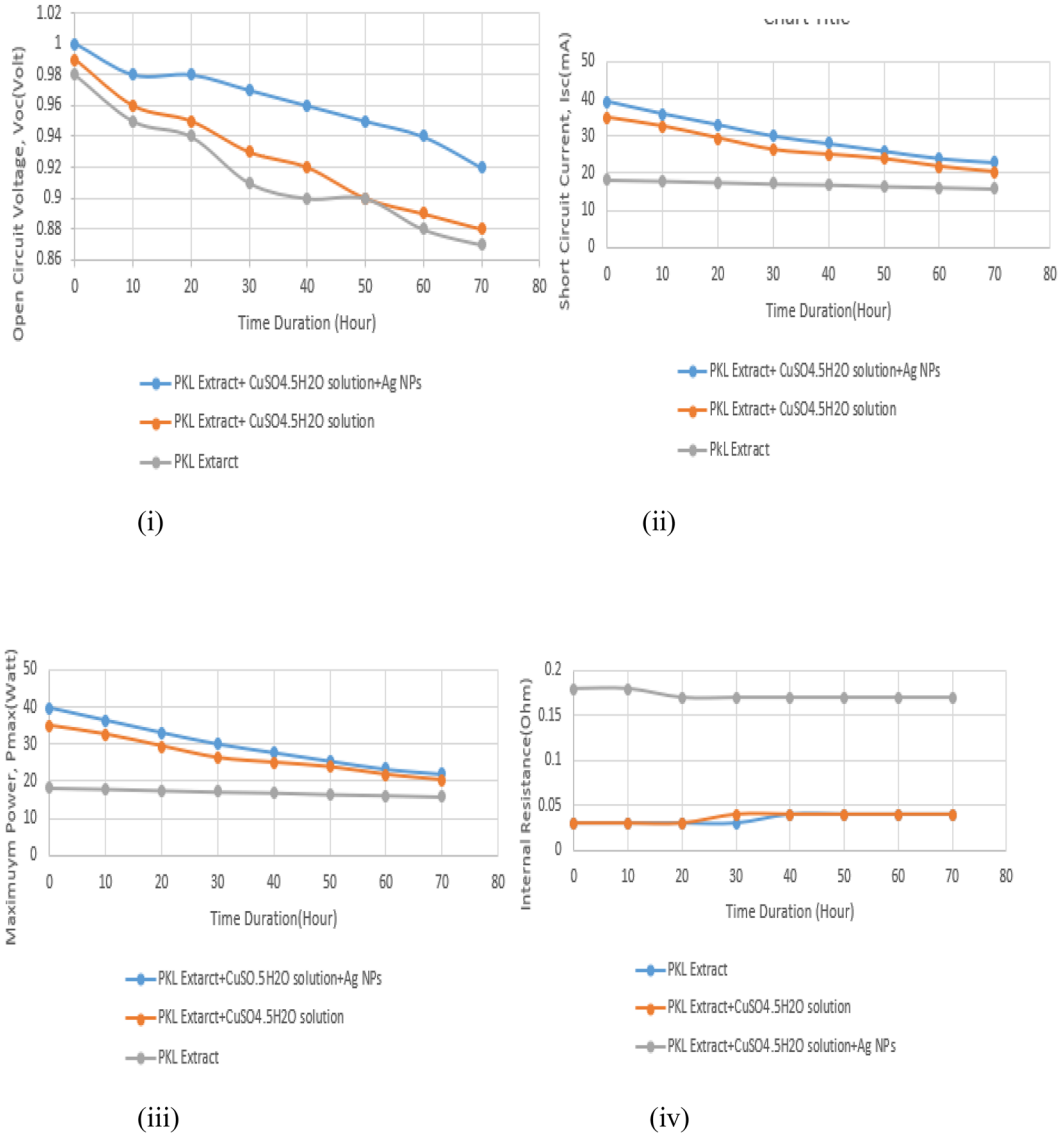

FIG. 8. PKL bio-electrochemical cell electrical activities: (i) open circuit voltage; (ii) short circuit current; (iii) maximum power; (iv) internal resistance.

IV. CONCLUSIONS

In this work, a straightforward, cheap, and environmentally sustainable biological approach for manufacturing Ag nanoparticles utilizing Pathor Kuchi Leaf extract has been devised. Several methods were used to characterize the Ag nanoparticles produced through biosynthesis. From the Scherrer equation, we calculate that the crystallite size of Ag nanoparticles with a spherical shape is 19 nm and was produced by biological means. Additionally, Ag nanoparticle FTIR spectra were revealed. Ag NPs' UV–Vis spectra revealed a maximum absorption at 400 nm, proving that Ag ions were bio-reduced to Ag NPs. The morphological characterization revealed dispersed spherical Ag NPs with an average particle size of 5 μm. Despite other research that been published on the green synthesis of silver nanoparticles using various plant extracts and their antibacterial effects, this work is the first to report on the role of Ag NPs in the development and lifespan of power generation in the bio-electrochemical cell. In summary, green-produced Ag NPs might help improve the power output of BPL bio-electrochemical cells. This research will pave the way for bio-electrochemical cells to generate power.

ACKNOWLEDGMENTS

The authors acknowledge Dr. A. A. Mamun and Dr. S. Sultana for their guidance and encouragement.

AUTHOR DECLARATIONS

Conflict of Interest

The authors have no conflicts to disclose.

Author Contributions

N. Y. Tanisa: Investigation (equal); Methodology (equal); Writing – original draft (equal); Writing – review & editing (equal). **Md Kamrul Alam khan**: Methodology (equal); Supervision (equal); Writing – review & editing (supporting). **M. Salahuddin**: Supervision (equal).

DATA AVAILABILITY

Data sharing is not applicable to this article as no new data were created or analyzed in this study.

REFERENCES

[1] K. A. Khan, S. Islam, S. R. Rasel, M. A. Saime, S. Hossain, and M. A. Rahman, Inf. Manage. Comput. Sci. **3**(2), 30–37 (2020).
[2] K. A. Khan, S. Paul, M. S. Rahman, R. K. Kundu, M. M. Hasan, M. Moniruzzaman, and M. A. Mamun, in *7th Power India International Conference (PIICON)* (IEEE-Publishing, 2016).
[3] A. Nirmala Grace and K. Pandian, Colloids Surf., A **297**, 63–70 (2007).
[4] K. A. Khan, M. H. Bakshi, and A. A. Mahmud, Am. J. Phys. Chem. **3**(5), 77–83 (2014).
[5] K. A. Khan, R. Akhlaqur, R. M. Siddikur, T. Anika, J. M. Kazi, and P. Shuva, in IEEE Innovative Smart Grid Technologies - Asia (ISGT-Asia), 2016.
[6] S. Raj, S. Chand Mali, and R. Trivedi, Biochem. Biophys. Res. Commun. **503**, 2814–2819 (2018).
[7] B. Khodadadi, M. Bordbar, A. Yeganeh-Faal, and M. Nasrollahzadeh, J. Alloys Compd. **719**, 82–88 (2017).
[8] N. Roy, A. Gaur, A. Jain, S. Bhattacharya, and V. Rani, Environ. Toxicol. Pharmacol. **36**, 807–812 (2013).
[9] M. Darroudi, M. Bin Ahmad, A. H. Abdullah, and N. A. Ibrahim, Int. J. Nanomed. **6**(1), 569 (2011).
[10] M. Ahamed, M. A. Majeed Khan, M. K. J. Siddiqui, M. S. AlSalhi, and S. A. Alrokayan, Physica E **43**(6), 1266–1271 (2011).
[11] Y. He, F. Wei, Z. Ma, H. Zhang, Q. Yang, B. Yao, Z. Huang, J. Li, C. Zeng, and Q. Zhang, RSC Adv. **7**, 39842–39851 (2017).
[12] A. Danagoudar, P. G K, M. Shantaram, B. Chatterjee, K. Ghosh, S. R. Kanade, and C. G. Joshi, "Cancer cell specific cytotoxic potential of the silver nanoparticles synthesized using the endophytic fungus, *Penicillium citrinum* CGJ-C2," Mater. Today Commun. **25**, 101442 (2020).
[13] F. Gol, A. Aygün, A. Seyrankaya, T. Gür, C. Yenikaya, and F. Sen, Mater. Chem. Phys. **250**, 123037 (2020).
[14] M. A. Hossain, B. Paul, K. A. Khan, M. Paul, M. A. Mamun, and M. E. Quayum, Mater. Chem. Phys. **282**, 125943 (2022).
[15] Y. Cui and C. M. Lieber, Science **291**, 851–853 (2001).
[16] T. Tuutijärvi, J. Lu, M. Sillanpaa, and G. Chen, J. Hazard. Mater. **166**(2–3), 1415–1420 (2009).
[17] K. Tanabe, Mater. Lett. **61**(23–24), 4573–4575 (2007).
[18] J. Huang, Q. Li, D. Sun, Y. Lu, Y. Su, X. Yang, H. Wang, Y. Wang, W. Shao, and N. He, Nanotechnology **18**, 105104 (2007).
[19] S. Prathap Chandran, M. Chaudhary, R. Pasricha, A. Ahmad, and M. Sastry, Biotechnol. Prog. **22**(2), 577–583 (2006).
[20] G. V. White, P. Kerscher, R. M. Brown, J. D. Morella, W. McAllister, D. Dean, and C. L. Kitchens, J. Nanomater. **2012**, 730746.
[21] S. Li, Y. Shen, A. Xie, X. Yu, L. Qiu, L. Zhang, and Q. Zhang, Green Chem. **9**, 852–858 (2007).
[22] S. Iravani, Green Chem. **13**, 2638 (2011).
[23] M. Shahriary, H. Veisi, M. Hekmati, and S. Hemmati, Mater. Sci. Eng.: C **90**, 57–66 (2018).
[24] P. Tippayawat, N. Phromviyo, P. Boueroy, and A. Chompoosor, PeerJ **4**, e2589 (2016).
[25] P. Rauwel, E. Rauwel, S. Ferdov, and M. P. Singh, Adv. Mater. Sci. Eng. **2015**, 624394.
[26] D. Garibo, H. A. Borbon-Nunez, J. N. D. Deleon, E. García Mendoza, I. Estrada, Y. Toledano-Magana, H. Tiznado, M. Ovalle-Marroquin, A. G. Soto-Ramos, A. Blanco, J. A. Rodríguez, O. A. Romo, L. A. Chavez-Almazan, and A. Susarrey-Arce, Sci. Rep. **10**, 12805 (2020).
[27] M. C. Moulton, L. K. Braydich-Stolle, M. N. Nadagouda, S. Kunzelman, S. M. Hussaina, and R. S. Varma, Nanoscale **2**(5), 763–770 (2010).
[28] A. P. Ajaykumar, A. Mathew, A. P. Chandni, S. R. Varma, K. N. Jayaraj, O. Sabira, V. A. Rasheed, V. S. Binitha, T. R. Swaminathan, V. S. Basheer, S. Giri, and S. Chatterjee, Antibiotics **12**(3), 564 (2023).
[29] M. Naveed, B. Bukhari, T. Aziz, S. Zaib, M. A. Mansoor, A. A. Khan, M. Shahzad, A. S. Dablool, M. W. Alruways, A. A. Almalki, A. S. Alamri, and M. Alhomrani, Molecules **27**, 4226 (2022).
[30] S. Elhawary, H. EL-Hefnawy, F. A. Mokhtar, M. Sobeh, E. Mostafa, S. Osman, and M. El-Raey, Int. J. Nanomed. **15**, 9771–9781 (2020).
[31] F. Azmi, D. Sispriatna, K. Ikhsan, M. Masrura, S. Azzahra, S. Mahidin, and M. D. Supardan, IOP Conf. Ser.: Mater. Sci. Eng. **334**(1), 012053 (2018).
[32] M. Jose, P. Sienkiewicz, K. Szymańska, D. Darowna, D. Moszyński, Z. Lendzion-Bielun, K. Szymanski, and S. Mozia, Nanomaterials **9**(5), 795 (2019).
[33] S. K. Shrivastava, A. Kulshreshtha, S. Srivastava, and R. K. Gangwar, Mater. Today: Proc. **62**(6), 4440–4444 (2022).
[34] N. Jayaprakash, J. J. Vijaya, K. Kaviyarasu, K. Kombaiah, L. J. Kennedy, R. J. Ramalingam, M. A. Munusamy, and H. A. Al-Lohedan, J. Photochem. Photobiol., B **169**, 178–185 (2017).
[35] S. Jebril, R. Khanfir Ben Jenana, and C. Dridi, Mater. Chem. Phys. **248**, 122898 (2020).
[36] S. Aslany, F. Tafvizi, and V. Naseh, Mater. Today Commun. **24**, 101011 (2020).
[37] E. Turunc, R. Binzet, I. Gumus, G. Binzet, and H. Arslan, Mater. Chem. Phys. **202**, 310–319 (2017).
[38] M. Mosaviniya, T. Kikhavani, M. Tanzifi, M. Tavakkoli Yaraki, P. Tajbakhsh, and A. Lajevardi, Colloid Interface Sci. Commun. **33**, 100211 (2019).
[39] S. O. Aisida, K. Ugwu, P. A. Akpa, A. C. Nwanya, U. Nwankwo, S. S. Botha, P. M. Ejikeme, I. Ahmad, M. Maaza, and F. I. Ezema, Surf. Interfaces **17**, 100359 (2019).
[40] M. B. Ananda, F. A. Sanjaya, T. Bachrurozy, H. M. Ar Rasyid, A. Barlian, A. H. Aimon, F. Qulub, P. Widiyanti, and A. Wibowo, Indones. J. Chem. **23**(2), 395 (2023).
[41] M. Tesfaye, Y. Gonfa, G. Tadesse, and S. Periyasamy, Heliyon **9**(6), e17356 (2023). Melakuu Tesfaye, Yodahe Gonfa, Getachew Tadesse, Tatek Temesgen, Selvakumar Periyasamy, and P. Shuva, Heliyon **9**(6), e17356 (2023).
[42] B. Paul, M. A. A. Mamun, A. Haque, M. Paul, and K. Ghosh, IEEE Trans. NanoBiosci. **18**, 490–497 (2019).
[43] M. A. Siddiquee, M. ud din Parray, S. H. Mehdi, K. A. Alzahrani, A. A. Alshehri, M. A. Malik, and R. Patel, Mater. Chem. Phys. **242**, 122493 (2020).
[44] K. Anandalakshmi, J. Venugobal, and V. Ramasamy, Appl. Nanosci. **6**, 399–408 (2016).
[45] P. Das, K. Ghosal, N. K. Jana, A. Mukherjee, and P. Basak, Mater. Chem. Phys. **228**, 310–317 (2019).
[46] R. Parameshwaran, S. Kalaiselvam, and R. Jayavel, Mater. Chem. Phys. **140**, 135–147 (2013).

[47]D. Kalpana and Y. S. Lee, Enzyme Microb. Technol. **52**, 151–156 (2013).
[48]N. Aziz, M. Faraz, R. Pandey, M. Shakir, T. Fatma, A. Varma, I. Barman, and R. Prasad, Langmuir **31**, 11605–11612 (2015).
[49]V. S. Suvith and D. Philip, Spectrochim. Acta, Part A **118**, 526–532 (2014).
[50]S. Hamedi, S. A. Shojaosadati, and A. Mohammadi, J. Photochem. Photobiol., B **167**, 36–44 (2017).
[51]S. Panja, I. Choudhuri, K. Khanra, and B. Ranjan Pati, Nano Biomedicine and Engineering **12**(1), 104–113 (2020).
[52]C. Wu, X. Zhou, and J. Wei, Nanoscale Res. Lett. **10**(1), 354 (2015).